DOE/NASA/0183-1
NASA CR-165327

Fuel Quality/Processing Study

Volume I: Final Report

J. B. O'Hara, A. Bela, N. E. Jentz, H. T. Syverson, H. W. Klumpe,
R. E. Kessler, H. T. Kotzot, and B. I. Loran
The Ralph M. Parsons Company

April 1981

Prepared for
NATIONAL AERONAUTICS AND SPACE ADMINISTRATION
Lewis Research Center
Under Contract DEN 3-183

for
U.S. DEPARTMENT OF ENERGY
Fossil Energy
Office of Coal Utilization

DISCLAIMER

DOE/NASA/51040-38
NASA TM-82824

DOE/NASA/51040--38

DE82 014953

Effect of Oxide Films on Hydrogen Permeability of Candidate Stirling Heater-Head Tube Alloys

Susan R. Schuon and John A. Misencik
National Aeronautics and Space Administration
Lewis Research Center
Cleveland, Ohio 44135

Work performed for
U.S. DEPARTMENT OF ENERGY
Conservation and Renewable Energy
Office of Vehicle and Engine R&D
Washington, D.C. 20545
Under Interagency Agreement DE-AI01-77CS51040

Prepared for
One hundred and tenth Annual Meeting of the
American Institute of Mining, Metallurgical, and Petroleum Engineers
Chicago, Illinois, February 22-26, 1981

EFFECT OF OXIDE FILMS ON HYDROGEN PERMEABILITY OF CANDIDATE STIRLING ENGINE HEATER-HEAD TUBE ALLOYS

by Susan R. Schuon and John A. Misencik

National Aeronautics and Space Administration
Lewis Research Center
Cleveland, Ohio

SUMMARY

High pressure hydrogen has been selected as the working fluid for the developmental automotive Stirling engine. Containment of the working fluid during operation of the engine at high temperatures and at high hydrogen gas pressures is essential for the acceptance of the Stirling engine as an alternative to the internal combustion engine. Most commercial alloys are extremely permeable to pure hydrogen at high temperatures. A program was undertaken at NASA Lewis Research Center (LeRC) to reduce hydrogen permeability in the Stirling engine heater head tubes by doping the hydrogen working fluid with CO or CO_2. Small additions of these gases were shown to form an oxide on the inside tube wall and thus reduce hydrogen permeability. This report summarizes a study of the effects of dopant concentration, alloy composition, and effects of surface oxides on hydrogen permeability in candidate heater head tube alloys.

Results showed that hydrogen permeability was similar for iron-base alloys (N-155, A286, IN800, 19-9DL, and Nitronic 40), cobalt-base alloys (HS-188) and nickel-base alloys (IN718). In general, the permeability of the alloys decreased with increasing concentration of CO or CO_2 dopant, with increasing oxide thickness, and decreasing oxide porosity. At high levels of dopants, highly permeable liquid oxides formed on those alloys with greater than 50 percent Fe content. Furthermore, highly reactive minor alloying elements (Ti, Al, Nb, and La) had a strong influence on reducing hydrogen permeability.

E-1176

INTRODUCTION

Hydrogen diffuses through metals very rapidly and is known to adversely effect their mechanical properties. Recently, investigators of the automotive Stirling engine have been exploring the use of hydrogen as a high efficiency working fluid. The successful use of hydrogen in such a system depends on the development of a means for reducing high pressure hydrogen permeation of hot components and thus gradual loss of the working fluid.

In the automotive Stirling engine[1], heat is transferred from the combustion gases through the external surface of thin-walled metal tubes to an internal hydrogen working fluid. Hydrogen must be contained in these "heater-head" tubes at pressures up to 21 MPa and temperatures up to 870° C for about 175 hours between refilling in order to make the Stirling engine concept technically and economically feasible. The purpose of this study, in support of the DOE-NASA Stirling Engine Highway Vehicle Systems Program, was to try to improve hydrogen containment in iron, cobalt, and nickel tubing alloys by promoting inside wall oxidation through the addition of small amounts of carbon monoxide and carbon dioxide to the hydrogen.

Although pure metals have a wide range of permeability to hydrogen[2], iron and nickel base alloys fall within a very narrow permeability range. Numerous studies have shown that ceramic and glass materials are many times less permeable to hydrogen than metals[4,5]. Misencik has shown that commercial alloys exposed to hydrogen containing impurities have a lower permeability to hydrogen than the same alloys exposed to high purity hydrogen[3]. Although it is generally known that some oxides are more effective permeability barriers than others, little is known about the effect of physiochemical differences of oxide scales on their permeability to hydrogen. Even less is known about the interaction effects of hydrogen and CO/CO_2 on the development of internal wall oxide barriers as well as on external scales in a multilayer system such as an oxidized heater head tube.

EXPERIMENTAL PROCEDURE

Seven commercial tubing alloys with an outside diameter of 4.8 mm and an inside diameter of 3.2 mm were investigated. Chemical analysis of the alloys (N155, A286, IN800, 19-9DL, Nitronic 40, HS188 and IN718) are reported in table I. These alloys vary considerably in their compositions, mechanical properties, and corrosion resistance. N155, which contains 20 percent CO, is used for the "heater head" tubing in the current developmental Stirling engine. The iron base alloys (A-286, IN800, 19-9DL, and Nitronic 40) were chosen as potential substitutes for N-155 which contains a high concentration of the strategic metal cobalt. The cobalt base alloy (HS188) and the nickel base alloy (IN718) were chosen to determine if alloy-base plays a major role in oxide film formation.

After fabrication into hairpin tubes, the permeabilities of these alloys to hydrogen and CO/CO_2 doped hydrogen were evaluated in a Stirling materials simulator rig as shown in figure 1 and as described by Misencik[3]. Prior to testing, each tube was leak-checked and then filled to 15 MPa with hydrogen and run for 105 hours in 5-hour cycles at 760° C. Diesel oil was used as the fuel in the Stirling test rig. The outside of the tubes was exposed to the combustion gases. After exposure to the external and internal gases, the tubes developed outside wall oxides and inside wall oxides as shown in figure 2.

Several test gases were used to obtain permeability data. Ultra high-purity hydrogen (<1 ppm O_2) was used to obtain permeability data for the case where no inside wall oxide (hereafter called inside oxide) was present representing a two-layer, metal wall-outside wall oxide (hereafter called outside oxide) system. Commercial purity hydrogen (364 to 526 ppm O_2), and 0.2 percent CO, 0.5 percent CO, 1 percent CO, 5 percent CO, 1 percent CO_2, 2 percent CO_2 and 5 percent CO_2 doped hydrogen were used to obtain data for inside oxide-metal wall-outside oxide systems. Permeability data for the alloys without oxides was obtained from a DOE-NASA study at IITRI[16].

After testing, the tubing was cut and the cross sections were analyzed by optical metallography. The thicknesses of the inside and outside oxide layers were measured directly on the metallograph as well as from subsequent optical micrographs. The inside and outside oxide surfaces were analyzed by optical and scanning electron microscopy (3,000X and 10,000X), X-ray diffraction, and energy-dispersive X-ray analysis.

RESULTS AND DISCUSSION

Results of the examination of the inside and outside oxide surfaces of the seven alloys are shown in figures 3 to 11. Figure 3 reflects relative Cr/Fe concentrations in the oxides. Figures 4(a) to (g) shows selected tube cross sections with both inside and outside oxide surfaces. Figures 5 to 11 are SEM photomicrographs illustrating oxide film morphology. Plots of permeability versus the partial pressure of oxygen in the doped hydrogen are shown in figure 12. Data for the base permeability of the metals were obtained from a DOE-NASA study at IITRI (ref. 16). Permeability and oxide thickness data from this study are shown in table II.

Fine Grained Oxide Formers

IN718

IN 718 tubes had the lowest permeability of the seven alloys in ultrapure hydrogen - 3.5×10^{-6} $cm^2/sMPa^{0.5}$. There was a greater than fifteen-fold decrease in permeability from IN718 exposed to hydrogen to IN718 exposed to 0.2 percent CO (table II).

IN718, a nickel-base alloy, developed a porous, fine-grained granular oxide in commercial purity hydrogen as shown in figure 5. As IN718 was exposed to increasing levels of CO or CO_2 dopant, the fine-grained granular oxide became less porous. In combustion gases, a thick granular outside oxide formed (fig. 5).

The thin inside oxide on IN718 and all other alloys appeared to be sesquioxides and were slightly enriched in Cr while the outside oxide exhibits substantial Cr enrichment as shown in figure 3(a). This alloy also contained higher levels of combined Al, Ti, and Nb than any other alloy (table I).

The thickness of the inside oxides ranged from about 1.5×10^{-4} cm to 3×10^{-4} cm. A thin outside oxide, 1.5×10^{-4} cm, developed on IN718 tubes filled with ultrapure hydrogen. When IN718 tubes were filled with hydrogen doped with 0.2 percent CO, the outside oxide thickness increased to 4×10^{-4} cm as shown in table II.

HS188

In ultrapure hydrogen, HS188 tubes have a permeability of 7.3×10^{-6} $cm^2/sMPa^{0.5}$. This is higher than the other alloys except N155 and 19-9DL. In 0.2 percent CO, the permeability was reduced to 2.9×10^{-6} $cm^2/sMPa^{0.5}$. There is a general reduction in the permeability of HS188 with increasing level of dopant in the hydrogen. At 5 percent CO, the permeability of HS188 is 0.5×10^{-6} $cm^2/sMPa^{0.5}$, a greater than ten-fold decrease in permeability compared to ultrapure H_2 data. However, with 5 percent CO_2, the permeability increased to 1.9×10^{-6} $cm/sMPa^{0.5}$.

This cobalt-base alloy, also developed a fine-grained granular oxide at all levels of dopant and in combustion gases as shown in figure 6. In commercial purity hydrogen (364 to 526 ppm O_2), HS188 developed a porous, granular inside oxide. At higher levels of dopant, this oxide became less porous. As with IN718, the inside and outside oxides of HS188 were enriched in Cr as shown in figure 3. This alloy was the only alloy evaluated that contained a rare earth - La.

The thickness of the inside and outside oxide varied little, ranging in thickness from 1.5×10^{-4} cm to 3.6×10^{-4} cm.

IN800

The permeability of IN800 tubes in pure H_2 was 4.4×10^{-6} $cm^2/sMPa^{0.5}$ and was reduced by the presence of an outside oxide. The permeability was further reduced when IN800 tubing was filled with doped hydrogen. At 0.2 percent CO, the permeability of IN800 was 1.1×10^{-6} $cm^2/sMPa^{0.5}$. There is a decrease in permeability with increasing level of dopant until at 5 percent CO, the permeability was 0.3×10^{-6} $cm^2/sMPa^{0.5}$. This represents over an order of magnitude reduction in H_2 permeability compared to ultrapure hydrogen.

A porous fine grained oxide was formed on IN800 in commercial purity hydrogen. IN800 was the only iron-base alloy which formed fine-grained granular oxides in CO/CO_2 and in the combustion gases as shown in figure 7. The ratio of Cr to Fe of the inside and outside oxides formed on IN800 was about 5 as shown in figure 3. This alloy had a relatively high Al plus Ti content.

The thickness of the inside oxide varies between 1.5×10^{-4} and 3×10^{-4} cm. The thickness of the outside oxide varied between 1.5×10^{-4} and 7.6×10^{-4} cm although the thickness was approximately 2×10^{-4} cm at most levels of dopant as shown in table II.

IN718, HS188 and IN800 formed fine-grained granular inside oxides at all levels of CO or CO_2 dopant. The permeability of these alloys decreased with increasing level of dopant i.e. PO_2 (See table II) as shown in figure 12. These alloys all had inside oxides which were enriched in Cr_2O_3. At low levels of CO or CO_2 dopant IN718, HS188, and IN800 developed porous fine-grained oxides (Figs. 5(a), 6(a), and 7(a)). As the level of dopant increased, a dense fine-grained oxide was formed which corresponded to the decreases in permeability.

The fine-grained oxide formers, IN718, HS188, and IN800, contained greater than 20 percent Ni. In hydrogen, these alloys range in permeability from 3.5×10^{-6} $cm^2/sMPa^{0.5}$ for IN718 (the lowest) to 7.3×10^{-6} $cm^2/sMPa^{0.5}$ for HS188 (3rd highest). After exposure to different levels of doped hydrogen, these alloys had permeabilities less than 1×10^{-6} $cm^2/sMPa^{0.5}$. IN718, which has higher levels of Ti, Nb, and Al, developed a low permeability at 0.2 percent CO. HS188, which has none of these reactive elements, develops a permeability less than $1 \times 10^{-6} cm^2/sMPa^{0.5}$ at 1 percent CO_2. HS 188 does, however, contain a small amount of La.

Coarse-Grained Oxide Formers

N155

The permeability of N155 without oxides (IITRI data ref. 16) is 1.8×10^{-5} $cm^2/sMPa^{0.5}$ which is higher than IN800, A286, or 19-9DL[2,16]. When the hydrogen filled tube was exposed to a combustion gas, the permeability was reduced to 7.8×10^{-6} $cm^2/sMPa^{0.5}$ which was less than 19-9DL. The permeability of N155 was reduced to 2.4×10^{-6} $cm^2/sMPa^{0.5}$ in 0.2 percent CO where a porous platy oxide formed. At higher levels of dopant, where a denser oxide formed, the permeability was reduced to between 1×10^{-6} and 2.1×10^{-6} $cm^2/sMPa^{0.5}$.

The type of oxide formed on N155 was highly dependent on the level of dopant in the hydrogen. In commercial purity hydrogen, N155 developed a thin oxide layer with small acicular crystals as shown in figure 8. Upon doping with 0.2 percent CO, N155 developed a coarse-grained platy oxide. A coarse-grained oxide was also formed in 1 percent CO, while a fine-grained granular oxide formed in 5 percent CO. When exposed to a combustion gas, N155 developed a dense anhedral outside oxide enriched in Cr_2O_3.

The inside oxide had a Cr to Fe ratio of about 1.5 while the outside oxide had a ratio of about 6. This alloy contains only Nb. It does not contain Ti or Al.

The inside oxide thickness varied between $1.5x10^{-4}$ and $4.0x10^{-4}$ cm. The outside oxide thickness varied between $1.5x10^{-4}$ and $6.6x10^{-4}$ cm. The thickness of the outside oxide formed on tubes filled with doped hydrogen is greater than the thickness of the outside oxide formed on tubes filled with ultrapure hydrogen.

Although N155 contains less than 50 percent Fe, it did not form a fine-grained granular oxide at high levels of dopant as did IN800. N155 contains higher levels of alloying elements such as Mo, Co, Mn, and Nb than IN800. These elements may enter into the oxide and strongly effect the development of the oxide. Due to the relatively thin oxides which form on these alloys, the relative presence of low concentration alloying elements in the scale was not readily measured.

Liquid Oxide Formers

Nitronic 40

In commercial purity hydrogen, Nitronic 40 developed a thin oxide layer. A coarse-grained blocky oxide similar to that formed on N155 developed in 0.2 percent CO. At higher levels of dopant, the blocky oxide melted as shown in figure 9 until at 5 percent CO_2, a "ropy" oxide was formed. This inside oxide showed evidence of cracking and spalling during thermal cycling.

Although the inside oxide melted at higher levels of dopant, the permeability of Nitronic 40 was consistantly low. At 0.2 percent CO, 0.5 percent CO, 1 percent CO and 5 percent CO, the permeability of Nitronic 40 was 0.3 cm /$sMPa^{0.5}$. At 0.5 percent CO_2, the permeability of Nitronic 40 was $0.6x10^{-6}$ $cm^2/sMPa^{0.5}$ (table II).

The inside oxide formed in doped hydrogen was enriched in Fe_2O_3. In contrast, the outside oxide was highly enriched in Cr as shown in figure 3. The very high Mn content of this alloy can be expected to promote Mn-rich spinels in the oxide scale.

The thickness of the inside oxide varied between $1x10^{-4}$ and $2.5x10^{-4}$ cm. The outside varied between $4x10^{-4}$ and 10^{-3} cm.

A286

The permeability of A286, when exposed to a combustion gas, was $5.5x10^{-6}$ $cm^2/sMPa^{0.5}$. When A286 tubes were filled with hydrogen doped with 0.2 percent CO, the permeability of A286 was reduced as a function of the level of dopant until the oxide melted at 5 percent CO and the permeability rose to $3.1x10^{-6}$ $cm^2/sMPa^{0.5}$.

A 286, formed a thin inside oxide in commercial purity hydrogen. While in 0.2 percent CO, A286 formed a dense granular oxide as shown in figure 10. There was evidence of melting at 0.2 percent CO. At 5 percent CO_2, extensive globular oxides indicated wide-spread melting. In contrast, A286 formed a thick, complex outside oxide in a combustion gas as shown in figure 10.

Figure 3 shows that the inside oxide was enriched in Fe while the outside oxide was enriched in Cr. This alloy contains only Ti as a reactive element - no Al or Nb.

In general, the thickness of the inside oxide increased as a function of the level of dopant. The outside oxide varied in thickness from 4.5×10^{-4} cm to 4.6×10^{-3} cm as shown in table II.

19-9DL

The permeability of H_2 in 19-9DL was 1.4×10^{-5} $cm^2/sMPa^{0.5}$ 16. When commercial hydrogen filled tubes were exposed to a combustion gas, the permeability was reduced to 8.1×10^{-6} $cm^2/sMPa^{0.5}$. This reduction in permeability was less than in IN800, N155, or A286. At 5 percent CO_2, the permeability of 19-9DL dropped to only 1.6×10^{-6} $cm^2/sMPa^{0.5}$.

Similar to Nitronic 40 and A286, 19-9DL formed a liquid oxide at higher dopant levels. In commercial purity hydrogen, a thin oxide was formed on the surface of the metal. The surface of the metal showed evidence of reaction with commercial hydrogen as shown in figure 11. In 5 percent CO_2, the oxide melted and formed discrete drops on the surface of a thin oxide layer. A dense oxide formed in a combustion gas as shown in figure 11(c).

The inside oxide on 19-9DL was enriched in Fe while the outside oxide was enriched in Cr_2O_3 (fig. 3). This alloy contained only minor amounts of Ti and Nb. Most of the Nb is tied up in the carbides.

Figure 12 shows the effects of oxygen partial pressure (dopant level) within the tubes on hydrogen permeability. For the fine grained, dense oxide formers, IN718, HS188, and IN800, permeability decreased with increasing oxygen partial pressure (figs. 12(a) to (c)).

Nitronic 40, A286, and 19-9DL form liquid oxides at high levels of dopant. Similar to fine-grained oxide formers, the hydrogen permeability initially decreased with increasing level of dopant. However, at higher dopant levels the oxides melted, and there was a rapid increase in permeability as shown in figures 12(d) and (e) for Nitronic 40 and A286 (19-9DL not shown but similar to A286). The inside oxides of liquid oxide forming alloys were enriched in Fe_2O_3. Nitronic 40, which has no Ti, Nb, or Al but has 9 percent Mn, developed a low permeability at 0.2 percent CO as shown in table II. Nitronic 40, A286, and 19-9DL all contain greater than 50 percent Fe. The weight fraction of other alloying elements varies from 7 percent in Nitronic 40 to 25 percent in A286. The presence of Al, Ti or Nb in liquid oxide forming alloys does not appear to be significant. While A286 has about 2 percent Ti, its permeability is high (table II) compared to Nitronic 40 which does not contain any of these elements (but does contain 9 percent Mn).

Alloying Effects

The permeability of an oxide is a function of the oxide porosity, structure, and its defect structure. Permeability of a metal can be reduced through the formation of a physical barrier such as an oxide or by trapping.

In this study the oxides which did not melt decreased in permeability with decreasing porosity and increasing level of dopant. If melting did occur, there was an increase in the permeability of the oxide. The permeability of one alloy composition over different levels of dopant compared to the permeability of a second alloy composition was strongly influenced by the minor alloying elements. While both Nitronic 40 and A286 increased in permeability with the formation of a liquid oxide, the magnitude of the permeability of Nitronic 40 was still lower than that of IN800, a fine-grained granular oxide former.

Alloying elements such as Mn, which would not be tied up in carbides could readily enter into the oxide, changing its lattice parameter or defect structure. Elements such as Mn, Al, and Si have a smaller ionic radius than Cr or Fe. When these elements enter into the sesquioxide, they reduce the lattice parameter of the oxide. This may reduce the permeability of hydrogen which moves through the oxide lattice as an interstitial.

At 2 percent CO, Nitronic 40, IN800, and HS188 formed fine-grained granular oxides. Nitronic 40 which has the highest level of combined Al + Mn + Si had the lowest permeability. IN800, which has an intermediate level of combined Al + Mn + Si had an intermediate permeability, while HS188 with no Al, Si, or Mn had the highest permeability. Kripyakevich, et. al[14] have found that the permeability of oxides formed on stainless steels changes as a function of the percentage of Al in the spinels.

Nb has a significant effect on the permeability of oxides. IN718, which has the highest level of Nb, also has the lowest permeability of the seven alloys. Recent unpublished research by Schuon at LeRC to reduce the hydrogen permeability in 19-9DL by selected alloy additions indicates that the addition of Nb to 19-9DL significantly reduces the pemeability of 19-9DL as based on hydrogen tests conducted for LeRC by IITRI (Bhattacharayya, 1981, personal communication). This may be due to potential trapping of hydrogen by niobium ions. The valence of niobium is five. When Nb occurs in a sesquioxide there would be a local charge imbalance which could trap hydrogen ions.

Effective Permeability Calculations

Two measures of the permeability of a material may be derived. The most common in the literature is the bulk permeability, ϕ, which expresses the overall permeability of a metal with possible surface oxides. The second is a calculated indication of the effective permeability of each individual oxide layer and in one case, the metal wall as well. The relationship between the measured bulk permeability and the effective permeability of the metal tube walls and the calculated permeability of inside and outside oxides is shown in figure 13 for IN800, N155, A286, and 19-9DL. (Data in ultra high purity H_2 and with no oxides formed were only available for these alloys from the test effort at IITRI (ref. 16)). The methodology for such calculations is presented in appendix A.

The calculated effective permeability of the outsides oxide for N155, IN800, and 19-9DL were of the same magnitude as shown in table III. The effective permeability of the outside oxide of A286 was ten times greater than that of the outside oxides on N155, IN800, or 19-9DL. The outside oxide formed on A286 was a complex, multilayer oxide which showed evidence of spalling.

The effective inside oxide permeability of A286 decreased sharply between 0.2 percent CO and 0.5 percent CO when a coherent oxide was formed. At 5 percent CO, the oxide melted and the effective permeability of the oxide increased to twice that of 0.2 percent CO.

The calculated effective inside oxide permeability of N155 varied as a function of the oxide morphology. At 0.2 percent CO where N155 developed a porous, platy oxide, the effective permeability was high as shown in table III. At 0.5 percent CO and 5 percent CO, the effective permeability was reduced by nearly a factor of six. Although the oxide formed in 0.5 percent CO had a much coarser grain size than that formed in 5 percent CO, the effective permeability of the oxides was similar (3.38×10^{-10} $cm^2/sMPa^{0.5}$ vs. 4.46×10^{-10} $cm^2/sMPa^{0.5}$).

In IN800, the effective oxide permeability decreased with increasing volume percent CO. There was a corresponding decrease in the porosity of the oxide layer with increasing volume percent CO or CO_2. There was no apparent change in the oxide grain size or shape.

Summary of Results

The effect of oxide characteristics on the hydrogen permeability of IN718, HS188, IN800, N155, Nitronic 40, A286, and 19-9DL tubing at 760° C was studied. The tubing was filled with hydrogen or CO/CO_2 doped hydrogen up to 15 MPa and exposed to an external combustion gas. It was observed that:

1. The bulk permeability of the alloys generally decreased with increasing volume percent CO or CO_2 dopant in the hydrogen (i.e. increasing partial pressure of oxygen) where no change occurred in the form of the oxide. The outside oxide thickness appeared to effect the bulk permeability but the effect was complicated due to apparent oxide spalling.

2. The hydrogen permeability of the alloys examined in doped H_2 was 19-9DL> N155> A286> HS188> IN800> Nitronic 40> IN718. In general, the permeability of an alloy to H_2 doped with CO or CO_2 was more strongly effected by the minor element composition - Al, Ti, Nb, or La - than by the major elements in the alloy.

3. Formation of a liquid oxide at high levels of dopant occurred in alloys with greater than 50 percent Fe (A286, Nitronic 40, and 19-9DL). Permeability rose with the formation of a liquid oxide.

4. The effect of hydrogen permeating through the metal effected the thickness of the outside oxide especially in Nitronic 40, IN718, A286, and N155 in CO and HS188 in CO_2.

5. The effective permeability of the outside oxide, a complex sesquioxide, remained about the same regardless of alloy composition except for the case of A286.

6. The grain size of the inside oxide was not as significant as the porosity of the oxide or the form of the oxide as far as affecting the effective permeability of the oxide as illustrated by N155. When the inside oxide did not melt the effective permeability decreased with decreasing oxide porosity and increasing P_{O}^{2} (levels of dopant).

APPENDIX A

Calculations of Effective Permeability

Diatomic gases can permeate through solids either as molecules or as interstitial solute atoms. The permeability rate may be described as:

$$\text{Nondissociative:} \quad J = \phi(P_1 - P_2)/t \tag{1a}$$

$$\text{or Dissociative:} \quad J = \phi \left(P_1^{1/2} - P_2^{1/2}\right)/t \tag{1b}$$

(where J = permeation rate, ϕ = permeability, P_1 = upstream gas pressure, P_2 = downstream gas pressure) depending on whether the gas molecule dissociates at the surface of the solid.[17]

Hydrogen permeation through ceramic materials has been assumed to be nondissociative although more recent studies have indicated that permeation through oxides is dissociative.[17,18] In dissociative permeation, the rate is determined by the time required for the hydrogen molecule to be absorbed on the surface of the material, dissociate and diffuse through the material.

Belyakov, et. al[6] have shown that below 450° C, desorption and dissociation effect the permeation rate in Kh18N10T, a stainless steel. In Stirling engine applications where the temperature is greater than 700° C, the activation energy for desorption and dissociation can be considered to be negligible.

For a tube, see figure 14, the permeation rate can be expressed as:

$$J = \phi 2\pi \ell_r \int_{r1}^{r2} \frac{r}{dr} \left(P_1^{1/2} - P_2^{1/2}\right) \tag{2}$$

where

r = radius
ℓ = tube length
P_1 = internal gas pressure
P_2 = external gas pressure
ϕ = permeability

or the permeation rate for the metal may be written:

$$J = \phi 2\pi \ell \frac{\left(P_1^{1/2} - P_2^{1/2}\right)}{\ln r2 - \ln r1} \tag{3}$$

In the Stirling materials simulator rig, the outside of the tubes is exposed to an oxidizing, burner-rig atmosphere and the inside is exposed to hydrogen with O_2, CO or CO_2 impurities in the gas. Therefore, both walls of the heater tubing tend to form oxides although they may differ in their effective permeability.

The permeation rate of each layer as shown in figure 14, may be expressed as:

$$\text{metal:}\quad Jm = 2\pi\ell\phi_m \frac{\left(P_2^{1/2} - P_3^{1/2}\right)}{\ln r3 - \ln r2} = g\left(P_2^{1/2} - P_3^{1/2}\right) \tag{4a}$$

$$\text{inside oxide:}\quad Jox_1 = 2\pi\ell\phi_{ox_1} \frac{\left(P_1^{1/2} - P_2^{1/2}\right)}{\ln r2 - \ln r1} = h_1\left(P_1^{1/2} - P_2^{1/2}\right) \tag{4b}$$

$$\text{outside oxide:}\quad Jox_2 = 2\pi\ell\phi_{ox_2} \frac{\left(P_3^{1/2} - P_4^{1/2}\right)}{\ln r4 - \ln r3} = h_2\left(P_3^{1/2} - P_4^{1/2}\right) \tag{4c}$$

At steady state permeation, the rates through the connected metal and oxides must be equal. Therefore:

$$Jox_1 = J_m = Jox_2 = J \tag{5}$$

and

$$h_1\left(P_1^{1/2} - P_2^{1/2}\right) = g\left(P_2^{1/2} - P_3^{1/2}\right) = h_2\left(P_3^{1/2} - P_4^{1/2}\right)$$

In the tubes $P_1 >> P_4$, therefore P_4 may be considered negligible.

An expression may be derived for hydrogen permeating through an oxide coated tube. From equation (5),

$$h_2 P_3^{1/2} = g\left(P_2^{1/2} - P_3^{1/2}\right) \tag{6}$$

or substituting equation (6) into equation (5),

$$Jm\text{-}ox_2 = \frac{gh_2}{(h_2 + g)} P_2^{1/2} \tag{7}$$

If, as in the case of the Stirling materials simulator rig, the tubes are coated on the inside and outside by different oxides,

$$Jox_1\text{-}m\text{-}ox_2 = h_1\left(P_1^{1/2} - P_2^{1/2}\right) \tag{8}$$

rearranging equation (7) and substituting into equation (8):

$$J = \frac{h_1 h_2 g}{[gh_2 + h_1 h_2 + gh_1]} P_1^{1/2} \tag{9}$$

It is possible to calculate the effective permeabilities of the inside and outside oxides from equations (4), (7), and (9).

This model assumes that only the outside oxide thickness increases with time. Although a change in outside oxide composition would effect this model, the change in composition appears to be negligible under the conditions of this study.

The permeability constant for four of the alloys studied here was determined in a DOE-NASA study at IITRI.[16] The permeability constant for the metal was substituted into equations (4) and (7) to determine the effective permeability constant of the outside oxide.

REFERENCES

1. J. R. Stephens, W. R. Witzke, G. K. Watson, J. R. Johntson, and W. R. Croft: NASA TM-73789, 1977.
2. R. W. Webb: NAA-SR-TDR 9844, 1964.
3. J. A. Miscencik: NASA TM-81578, 1980.
4. Yu. I. Belyakov, Yu. I. Zvezdin, and A. A. Kurdymov: Fiz.-Khim. Mekh. Mater., 1970, Vol. 6, pp. 37-39.
5. Yu. I. Archakov, Yu. I. Zvezdin, V. P. Kirillova, V. N. Malyshev, A. A. Nazarov, and E. P. Novakovskaya: Fiz.-Khim. Mekh. Mater., 1974, Vol. 10, pp. 92-95.
6. Yu. I. Belyakov, A. V. Ivanov, V. A. Kurakin, and A. A. Kurdyumov: Fiz.-Khim. Mekh. Mater., 1978, Vol. 14, pp. 39-42.
7. B. F. Kachmar, V. V. Fedorov, V. M. Sidorenko, and A. L. Bichuia: Fiz.-Khim. Mekh. Mater., 1976, Vol. 13, pp. 113-115.
8. R. A. Strehlow and H. C. Savage: Nucl. Technol., 1974, Vol. 22, pp. 127-137.
9. W. A. Swansiger, R. E. Musket, L. J. Weirick, and W. Bauer: J. Nucl. Mat., 1974, Vol. 53, pp. 307-312.
10. E. H. Van Deventer, T. A. Renner, R. H. Pelto, and V. A. Maroni: J. Nucl. Mater., 1977, Vol. 64, pp. 241-248.
11. R. G. Parkheta and V. I. Pokhmurski: Zashch Pokrytiya Met., 1976, Vol. 10, pp. 102-104.
12. W. A. Swansiger and R. Batasz: J. Nucl. Mater., 1979, Vol. 85-86, pp. 285-339.
13. E. H. Van Deventer, V. A. MacLaren, and V. A. Maroni: J. Nucl. Mater., 1980, Vol. 89, pp. 169-173.
14. R. I. Kripyakevich, Yu. I. Zvezdin, A. V. Guts, and I. V. Semchishin: Fiz.-Khim. Mekh. Mater., 1971, Vol. 7, pp. 47-51.
15. G. R. Caskey, Jr. and R. G. Derrick: Metall. Trans. A, 1977, Vol. 8A, pp. 511-513.
16. E. J. Vesely, Jr. Highway Vehicle Systems; pp. 86-98, CONF 791082, Department of Energy, Washington, D.C., 1979.
17. D. S. Shupe: J. Chem. Phys., 1978, Vol. 68, pp. 266-270.
18. J. T. Bell, J. D. Redman, and H. F. Bittner: Metall. Trans. A, 1980, Vol. 11A, pp. 775-782.

TABLE I. - COMPOSITION OF SEVEN COMMERCIAL ALLOYS

	Cr	Ni	Co	Mn	Mo	W	Ti	Nb	Si	Al	C	N	Fe	Other
N 155	21.2	19.9	19.0	1.45	3.03	2.61	-----	1.05	0.53	----	0.11	0.16	Bal	-----
A 286	14.4	24.7	-----	1.01	1.17	-----	2.12	----	.62	0.2	.06	----	↓	[a]0.58
IN 800	22.5	32.6	-----	.73	----	-----	.52	----	.53	.54	.01	----		-----
19-9DL	18.3	8.76	-----	1.02	1.26	1.13	.27	.37	.47	----	.29	----		[b].03
Nit. 40	20.8	7.02	.09	9.36	.03	-----	----	----	.49	----	.03	.34		-----
HS 188	22.0	22.0	40.0	----	----	14.0	----	----	----	----	.08			[c].08
IN 718	18.6	53.0	-----	.2	3.10	-----	.90	5.00	.30	.40	.04	----		-----

[a]Cu + V
[b]Cu
[c]La

TABLE II. - BULK PERMEABILITY AND OXIDE THICKNESS

	Ultra pure H2	0.2% CO	0.5% CO	1% CO	5% CO	0.5% CO_2	1% CO_2	2% CO_2	5% CO_2
	P_{O_2} (MPa)								
	-----	0.114	0.2851	0.56	2.851	0.36364	0.727	1.45	3.636
	Permeability [a]10^{-6} $cm^2/sMPa^{0.5}$								
HS 188	7.3	2.9	2.2	2.1	0.5	1.8	0.8	0.7	1.9
N 155	7.8	2.4	1.2	1.4	1.2	1.3	1.0	1.5	2.1
IN 800	4.4	1.1	1.0	1.4	.4	.8	.5	.4	.6
A 286	5.5	2.7	1.5	1.5	3.1	1.4	1.3	.7	2.7
Nitronic 40	-----	.3	.27	.3	.3	.6	.2	-----	-----
IN 718	3.47	.2	.2	.2	.1	.2	.2	.26	.71
19-90L	-----	---	-----	---	----	---	----	-----	1.6
	Inside oxide thickness [a]10^{-4} cm								
HS 188	-----	1.5	2.0		2.0	1.5	2.0	3.0	3.0
N 155	-----	2.5	2.0		1.0	1.5	3.6	4.1	4.3
IN 800	-----	1.5	2.5		2.5	2.5	3.0	2.0	3.0
A 286	-----	1.5	2.5		11.2	2.0	4.3	5.1	5.0
Nitronic 40	-----	2.0	2.5		1.0	1.0	2.0	-----	-----
IN 718	-----	2.0	1.5		2.0	2.0	2.5	3.0	3.0
19-90L	-----	---	-----		----	---	----	-----	2.5
	Outside oxide thickness [a]10^{-4} cm								
HS 188	1.5	3.0	2.5		1.5	1.5	3.6	3.6	4.0
N 155	1.5	3.0	3.6		5.6	1.5	5.0	6.6	7.0
IN 800	2.5	2.5	2.5		1.5	2.0	7.6	2.0	3.0
A 286	20.3	6.1	4.6		15.2	6.1	40.6	24.2	25.0
Nitronic 40	-----	4.0	4.0		10.2	5.0	5.0	4.1	-----
INC 718	1.5	4.0	4.0		10.2	5.0	5.0	4.1	4.1
19-90L	-----	---	-----		----	---	----	-----	-----

[a]Misencik, 1981 unpublished data.

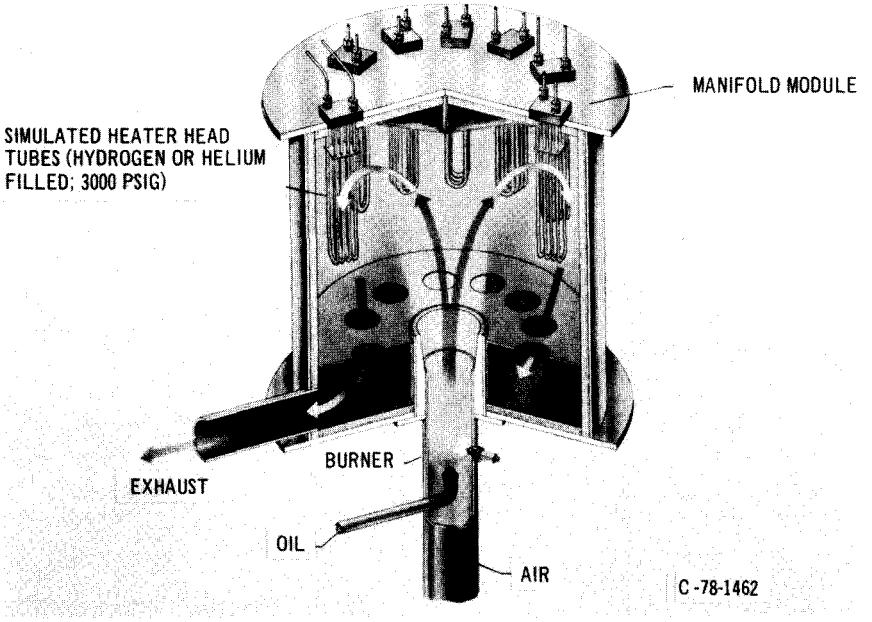

Figure 1. - Diagram of the Stirling Materials Simulator showing candidate heater head tubes.

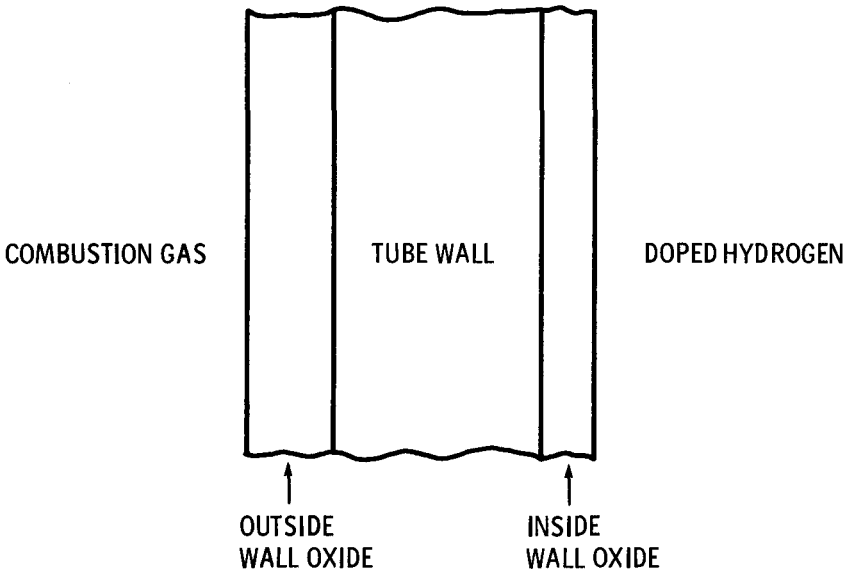

Figure 2. - Tubing cross section.

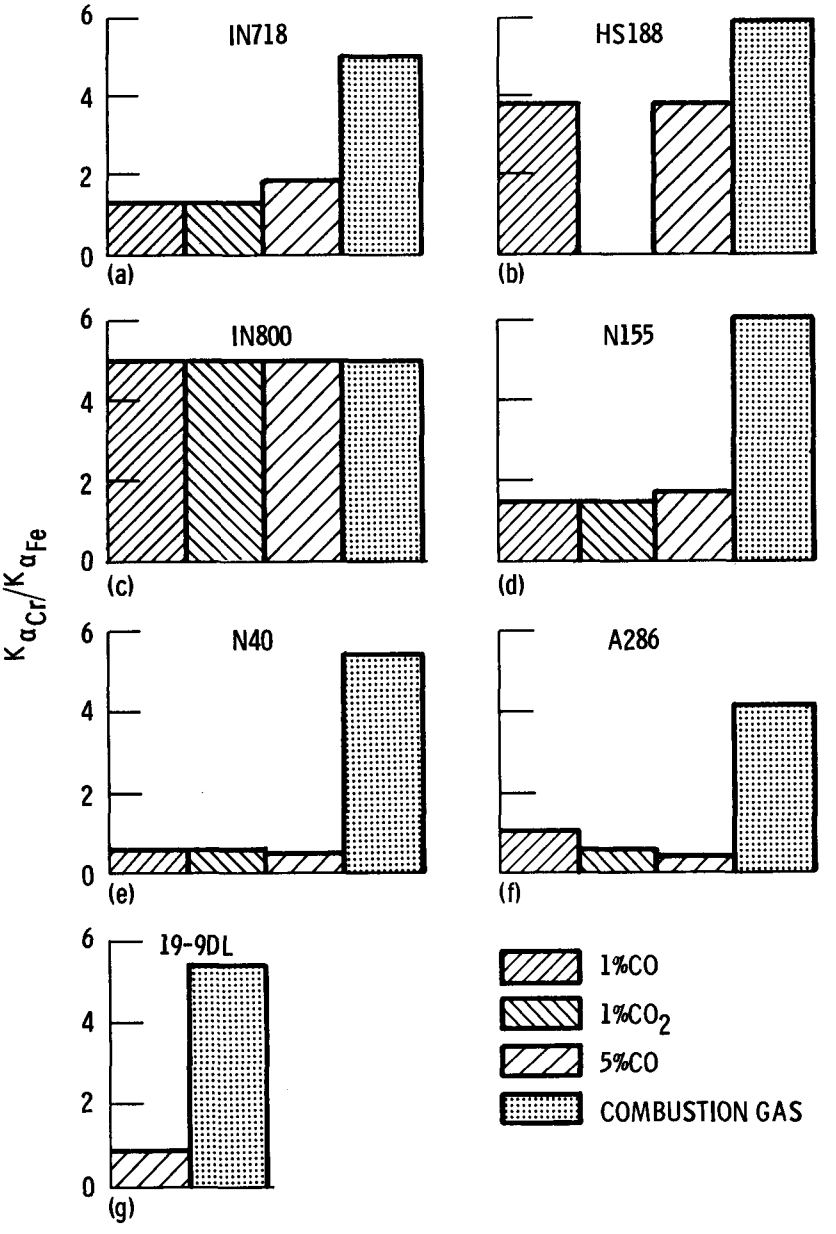

Figure 3. - Intensity of $K_{\alpha Cr}/K_{\alpha Fe}$ in oxides formed on seven commercial alloys (inside oxide - CO or CO_2 doped H_2 outside oxide - combustion gas).

OUTSIDE OXIDE IN718

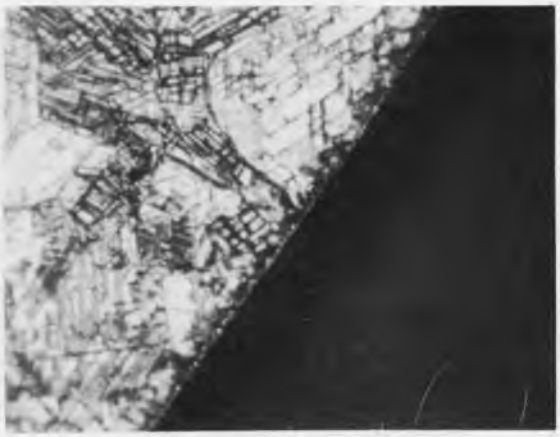

INSIDE OXIDE IN718

OUTSIDE OXIDE H5188

INSIDE OXIDE H5188

OUTSIDE OXIDE IN800

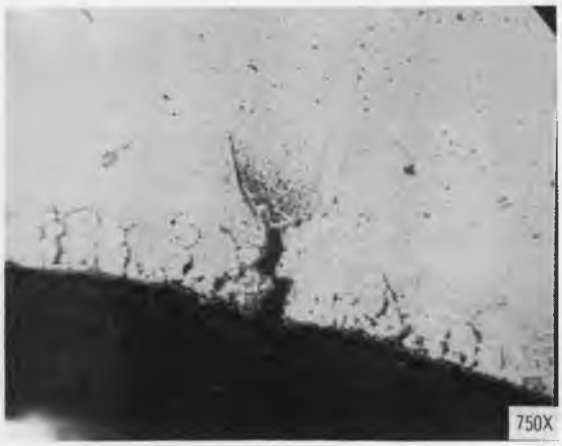

INSIDE OXIDE IN800

Figure 4. - Crossection of alloy tubing (inside filled with H_2+5%CO_2, outside exposed to combustion gas).

OUTSIDE OXIDE N155

INSIDE OXIDE N155

OUTSIDE OXIDE N40

INSIDE OXIDE N40

OUTSIDE OXIDE A286

INSIDE OXIDE A286

Figure 4. - Continued.

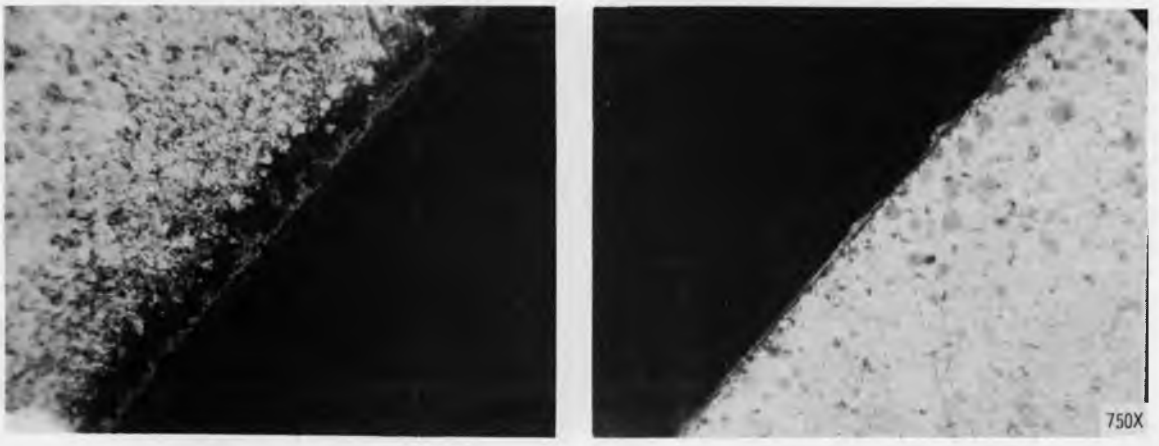

OUTSIDE OXIDE 19-9DL

INSIDE OXIDE 19-9DL

Figure 4. - Concluded.

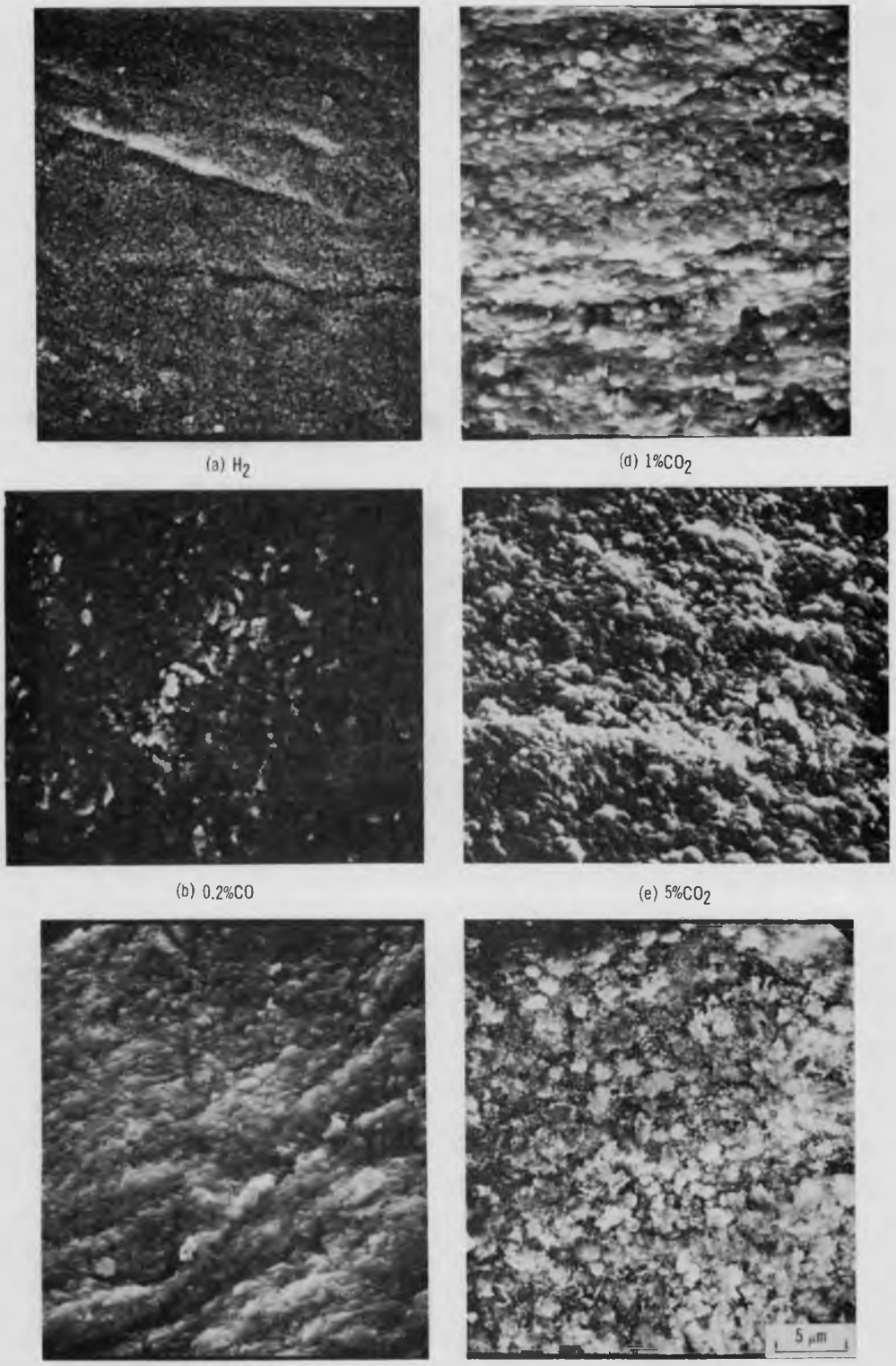

(a) H_2

(b) 0.2%CO

(c) 5%CO

(d) 1%CO_2

(e) 5%CO_2

(f) COMBUSTION GAS

Figure 5. - SEM photomicrographs of oxide surfaces formed on IN718.

(e) .5%CO_2

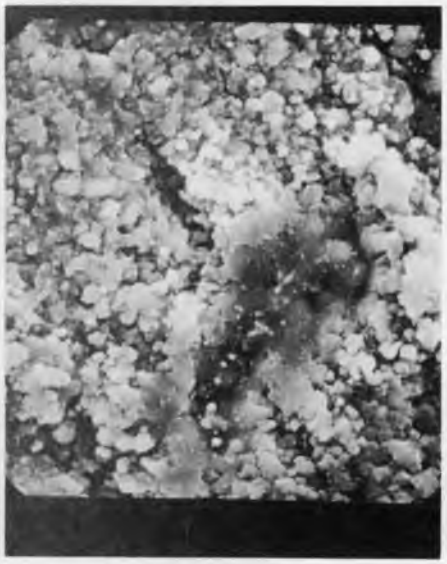

(f) 1%CO_2

(g) COMBUSTION GAS

Figure 6. - Concluded.

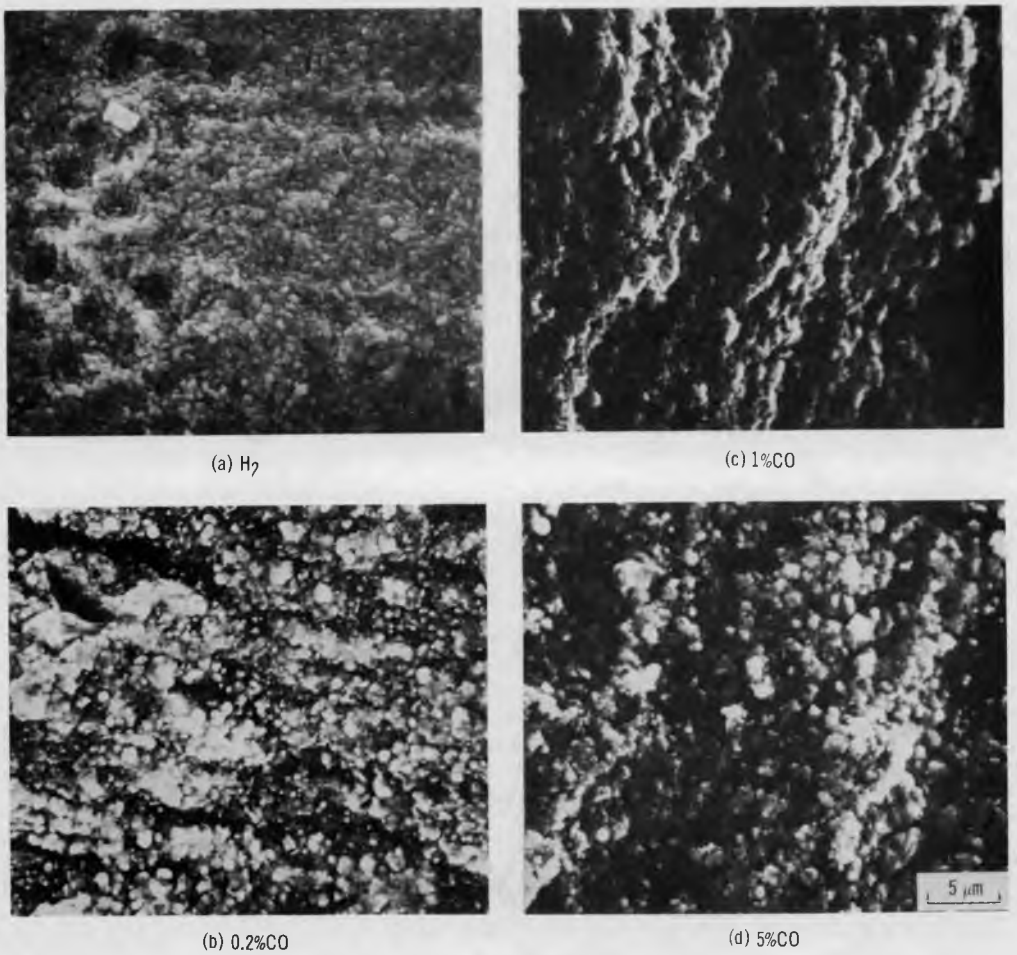

(a) H_2

(c) 1%CO

(b) 0.2%CO

(d) 5%CO

Figure 6. - SEM photomicrographs of oxide surfaces formed on HS188.

(a) H_2

(b) 1%CO

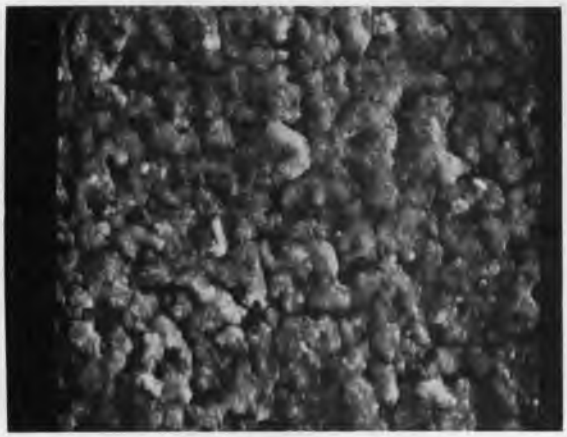

(c) 5%CO

(d) 1%CO_2

(e) COMBUSTION GAS

5 μm

Figure 7. - SEM photomicrographs of oxide surfaces formed on IN800.

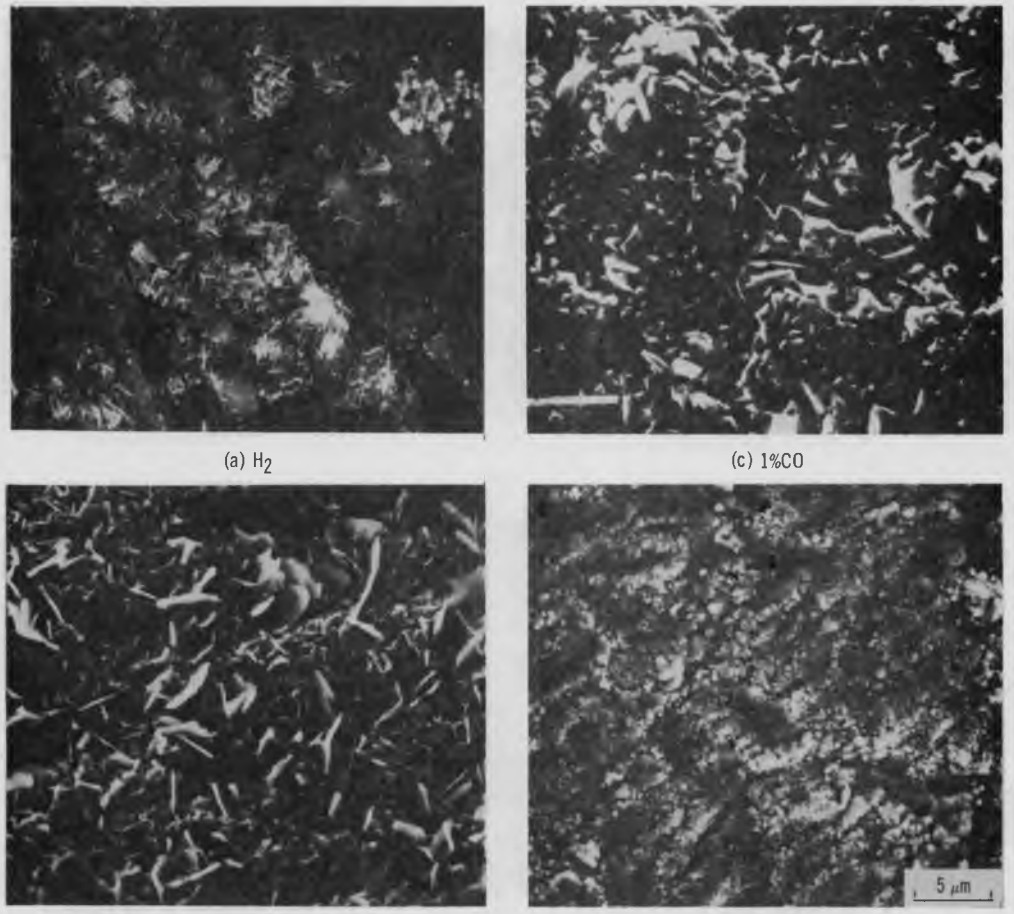

(a) H_2 (c) 1%CO

(b) 0.2%CO (d) 5%CO

Figure 8. - SEM photomicrographs of oxide surfaces formed on N155.

(e) .5%CO_2

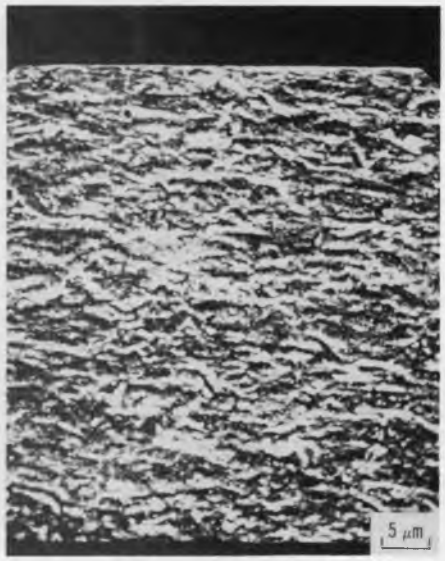

(f) 1%CO_2

(g) COMBUSTION GAS

Figure 8. - Concluded.

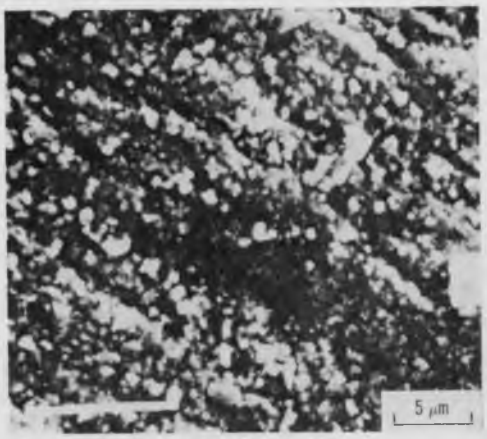

(a) H_2

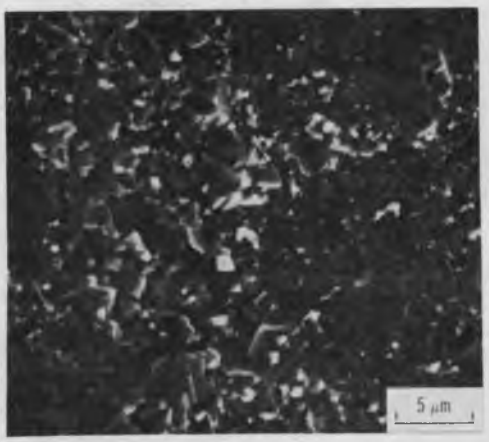

(b) 0.2%CO

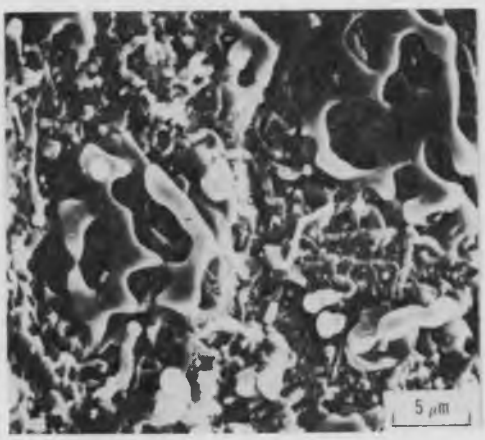

(c) 1%CO

(d) 5%CO

(e) 1%CO_2

Figure 9. - SEM photomicrographs of oxide surfaces formed on Nitronic 40.

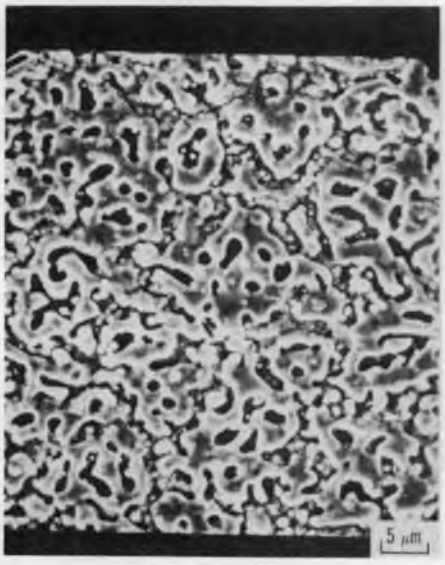

(f) 5%CO_2

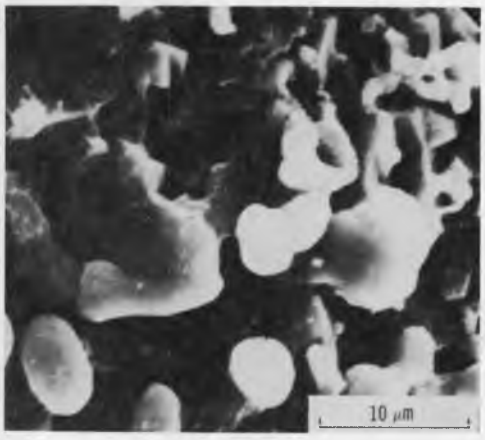

(h) 1%CO

(g) COMBUSTION GAS

Figure 9. - Concluded.

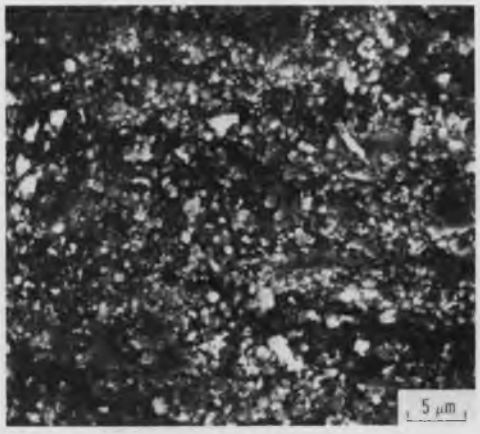

(a) COMMERCIAL H_2

(d) 1%CO

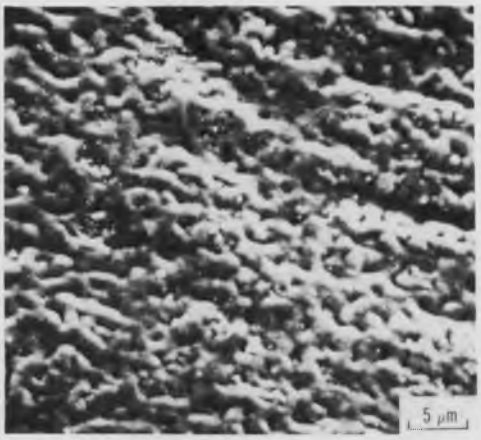

(b) 0.2%CO_2

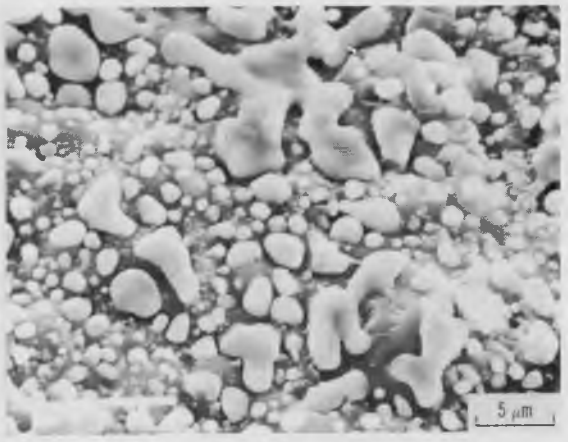

(e) 5%CO

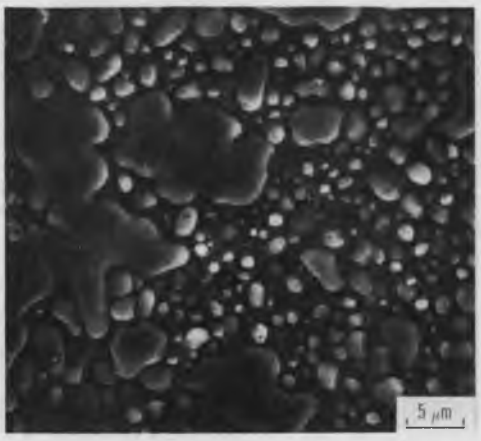

(c) 5%CO_2

(f) COMBUSTION GAS

Figure 10. - SEM photomicrographs of surface oxides formed on A286.

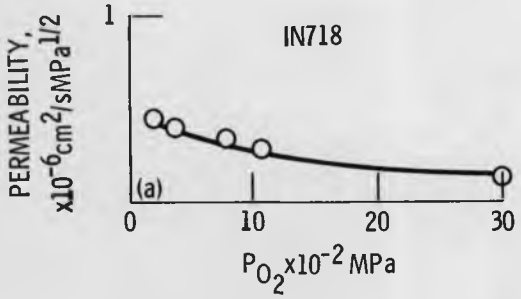

Figure 12. - Partial pressure of oxygen (level of Dopant) versus permeability in stirling heater-head tube candidate alloys.

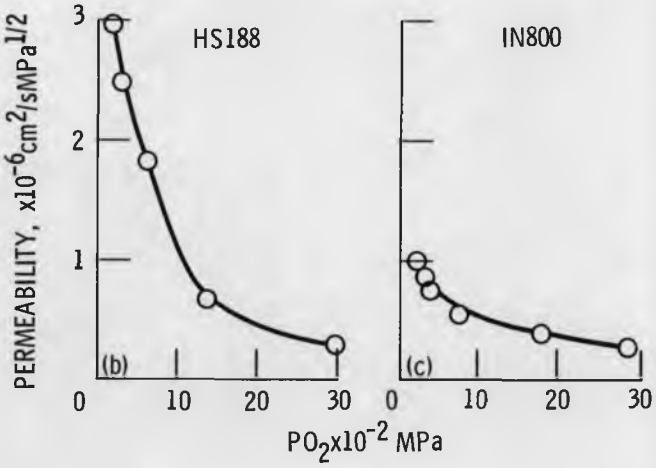

Figure 12. - Continued.

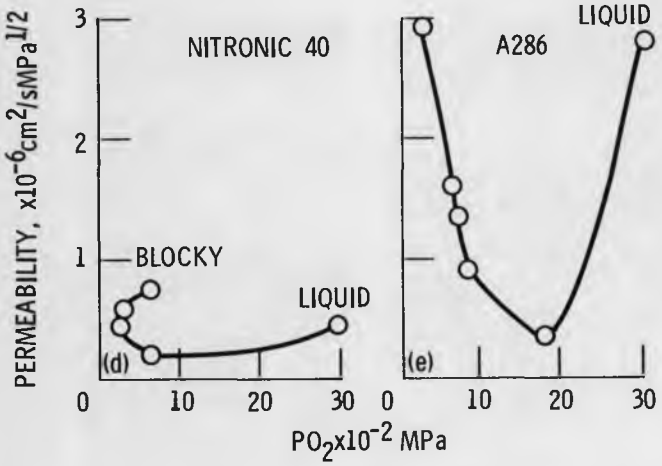

Figure 12. - Concluded.